Wind and Structures, *Vol. 29, No. 2 (2019) 111-127*
DOI: https://doi.org/10.12989/was.2019.29.2.111

Aerodynamics of tapered and set-back buildings using Detached-eddy simulation

Ashutosh Sharma[*1], Hemant Mittal[1a] and Ajay Gairola[2b]

[1]*Centre of Excellence in Disaster Mitigation and Management, Indian Institute of Technology Roorkee, Roorkee-247667, India*
[2]*Department of Civil Engineering, Indian Institute of Technology Roorkee, Roorkee-247667, India*

(Received March 24, 2018, Revised October 23, 2018, Accepted October 26, 2018)

Abstract. The tapered and set-back type of unconventional designs have been used earlier in many buildings. These shapes are aerodynamically efficient and offer a significant amount of damping against wind-induced forces and excitations. Various studies have been conducted on these shapes earlier. The present study adopts a hybrid approach of turbulence modelling i.e., Detached-eddy Simulation (DES) to investigate the effect of height modified tapered and set-back buildings on aerodynamic forces and their sensitivity towards pressure. The modifications in the flow field around the building models are also investigated and discussed. Three tapering ratios (T.R.= (Bottom width- Top width)/Height) i.e., 5%, 10%, 15% are considered for tapered and set-back buildings. The results show that, mean and RMS along-wind and across-wind forces are reduced significantly for the aerodynamically modified buildings. The extent of reduction in the forces increases as the taper ratio is increased, however, the set-back modifications are more worthwhile than tapered showing greater reduction in the forces. The pressure distribution on the surfaces of the buildings are analyzed and in the last section, the influence of the flow field on the forces is discussed.

Keywords: aerodynamic modification; tapering ratio; set-back; DES model; flow field

1. Introduction

A building submerged in turbulent boundary layer experiences loads and excitations in three directions and as the height of the building is increased the wind loads are enhanced (Kim *et al*. 2015, Zhao *et al*. 2011). The outer geometrical shape of the structure contributes majorly in providing resistance against wind-induced loads and excitations in either direction. The traditionally designed square, rectangular bluff shaped buildings are more likely to be confronted by wind-induced dynamic loads. The aerodynamic modifications are efficient ways to alleviate these loads. A comprehensive review on the potency of aerodynamic modifications of tall buildings has been presented by Sharma *et al. (*2018), Asghari *et al*. (2016). Other reviews by Kareem *et al.* (1999), Kareem (1983) also focus on the effectiveness of these treatments and moreover, Tamura research group has been exploring the behaviour of unconventional tall structures since the past decade and contributed appreciably in this field.

The aerodynamic modifications change the fashion in which the approaching wind interacts with the building and form vortices, in this way the mechanism of vortex shedding can be customized.

The frequency of vortex shedding highly depends on the width of the building and Strouhal number (*St*), the major modifications in the outer architecture of the buildings such as taper and set-back spread the vortex shedding frequency to a broader range throughout the height of the building (Xie 2014, Kareem 1983), which consequently breaks the coherency between the vortices and suppresses the dynamic forces and response (Kareem 1983, Irwin 2009, Kim and You 2002, Kim and Kanda 2010a, 2013). John Hancock Centre, Yokohama Tower etc have been adopted with the taper on two sides and The Petronas Tower (Kaula Lumpur), Jin Mao Tower (Shanghai) and Sear Tower (Chicago) have utilized set-back modification.

Previously many studies have analyzed the tapering and set-back modifications and its impact on wind-induced loads and responses. A summary and main findings of some studies are presented in the Table. 1. Among the literature presented in Table 1, (Kim and Kanda 2010a, 2013, Deng *et al*. 2015, 2018) discuss the pressure distribution on the surfaces of the building experimentally.

In past, (Meng *et al.* 2018, Zhao *et al.* 2017, Mou *et al*. 2017, Huang *et al.* 2007) have analyzed the pressure sensitivity on the surfaces of a tall building with the help of CFD. The Reynolds-average Navier-Stokes (RANS) and Large-eddy Simulation (LES) approaches have been employed in these studies. The RANS models are widely used at the industry level due to its capability to predict mean flow conditions with reasonable accuracy and lower computational cost (Tominaga 2009, Mochida 2008) but cannot provide the good results in cases of massively separated flows (Rodi 1997, Schmidt and Thiele 2002, Spalart 2009). On the other hand, the LES approach is capable of handling the complex turbulent flows

*Corresponding author, Researcher
E-mail: ashukridha@gmail.com
[a] Researcher
E-mail: hemantkiet@gmail.com
[b] Professor
E-mail: garryfce@gmail.com

http://www.techno-press.com/journals/was&subpage=7 ISSN: 1226-6116 (Print), 1598-6225 (Online)

Table 1 Summary and main findings of previous studies on major modifications

Reference	Method	Modification	Conclusions
Kim and You 2002	HFFB	5%, 10%, 15%,	Tapering is more effective for across-wind direction than along-wind direction, responses are not always reduced.
Kim *et.al.* 2008	Aeroelastic	5%, 10%, 15%	Tapering is beneficial for high-reduced frequencies with moderate damping ratios, increase in response for very low damping and high-velocity range.
Kim and Kanda 2010a	HFFB, SMPSS	5%, 10% tapered and set-back	Mean drag and fluctuating lift forces are reduced, the set-back model is more effective in reduction than tapered.
Kim and Kanda 2010b	HFFB	5%, 10% tapered and set-back	Mean along-wind and fluctuating across-wind OTM decrease significantly
Kim *et.al.* 2011	HFFB	5%, 10% tapered and set-back	Modified models with the mass centre and rigidity centre eccentricity have lesser along wind and torsional acceleration but across-wind acceleration is high, increase in eccentricity decreases across-wind acceleration and increases torsional acceleration.
Kim and Kanda 2013	SMPSS	5%, 10% tapered and set-back	The height of vortex formation moves upward, vortices shed more frequently in the upper region than lower region.
Deng *et.al.* 2015	SMPSS	2.2%, 4.4%, 6.6% taper	Reduction in across-wind response effectively, mitigation effect increases with an increase in taper ratio, vortex shedding frequency increases.
Kim *et.al.* 2015	Aeroelastic	10%	Responses of the tapered model are suppressed for low turbulence and urban flow environment but grid generated flow gives adverse results.
Deng et al. 2018	SMPSS	2.2%, 4.4%, 6.6% taper	The peak negative pressure is observed to be reduced with an increase in the tapering ratio.

satisfactorily (Murakami 1998, Rodi 1997, Huang *et al.* 2007) but good reversed flow prediction (Murakami 1993, Murakami and Mochida 1995). But LES is not an economical approach in terms of computational cost and time. The hybrid DES approach (Spalart 1997) offers lesser computational cost with the accuracy comparable to the LES model (Liu and Niu 2016, 2017).

Paik *et al.* (2009), Haupt *et al.* (2011) adopted the DES technique for flow field prediction and pressure distribution analysis around the cubes. Schmidt and Thiele (2002) examined and compared the efficacy of the RANS, LES and DES to capture the flow field around a cube and concluded that DES can reproduce flow features correctly. Yan and Li (2017) examined the accuracy of LES and DES for wind load estimation for a high rise structure and reported that DES predicts the mean pressure coefficient quite well as compared to experimental tests, but found some discrepancies in the prediction of negative pressure and a slight over-estimation of fluctuating components of pressure observed. Liu and Niu (2016), Liu *et al.* (2017) tested the SRANS, URANS, LES and DES models for flow prediction around a building model, and reported that all models could predict better mean flow approximation on windward side, however LES and DES models reproduced better transient and mean flow pattern on leeward and sides of the building. Although among all the models DES and LES can predict similar results in the wake region and the DES model requires a lesser number of grids. Sharma et al. 2019 investigated the effect of interference between two buildings on flow field with DES approach based on k-ω SST model. For the guidelines regarding the implementation of DES approach, Bunge *et al*. (2007) may be followed.

2. Objective

The earlier studies explored the wind-induced loads and dynamics of tapered and set-back buildings and practised the aerodynamic treatments on reference square building models by keeping height and base dimensions same, but these modifications may cost the usable floor area (as the volume of the building after modification is reduced), which can only be recompense by increasing the number of floors or by increasing the base area. Tse *et al.* (2009) identified this issue and investigated the influence of an increase in height of building to keep the volume same on the aerodynamic forces and overall cost associated with it. Majority of the past studies analyze the forces, moments acting on the modified buildings and dynamics of the structures, but very few discuss the pressure sensitivity of such buildings. Moreover, none of the previous studies discusses the modifications in the flow field due to modifications in the geometry.

Considering the above-mentioned gaps in earlier studies, the present work analyzes characteristics of wind forces and pressure distribution of taper and set-back buildings (at 0^{o} of wind incidence) by keeping the height of all the buildings same as that of reference square building and customizing the other dimensions to keep the volume of tall building same. To perform the numerical simulation of aerodynamically modified tapered and set back buildings, the modified version of DES i.e. DDES (Delayed detached-eddy simulation) approach based on SST $k-\omega$ model is adopted for the cases to predict the pressure distribution and flow field around the buildings. The results obtained from the CFD analysis were compared with wind tunnel test data for the validation of the turbulence model.

3. Methodology and CFD setup

The selected building models (Fig. 1) were first tested in a wind tunnel at Department of Civil Engineering, Indian Institute of Technology, Roorkee, India. The turbulent boundary layer having power law exponent (α) of 0.20 was simulated in the wind tunnel. The Reynolds Number (R_e) for present wind tunnel test based on the velocity at the top of the model U_H (9.6 m/sec) and model width B is 5.73 x 10^4. The wind forces were measured by 5-component load cell by NISSO (LMC-5511-10) (capacity: $F_x = F_y = 10\, kg, M_x = M_y = 4\, kg-m, M_z = 1\, kg-m$) and load cell was located at the bottom of the models (below the tunnel floor). A sampling frequency of 250 Hz is used with a sampling time 60 seconds and a low pass filter of 45 Hz was applied.

The angle of incidence varies from 0^0 to 45^0 with an interval of 5^0. The obtained results later used to validate the turbulence model. The velocity and turbulence profiles simulated in the wind tunnel are shown in the later in section 3.3 (Fig. 4).

The Standard DES model can behave imprecisely in the regions of the thick boundary layer and shallow separation regions if LES mode of DES gets activated in the attached boundary layer region. This phenomenon ultimately causes factitious separation of the flow in laminar like fashion termed as 'Modeled Stress Depletion' (Spalart 2006). Menter and Kuntz 2004, Strelets 2001 have proposed amendments in DES approach i.e., DDES (Delayed Detached-eddy Simulation) to rectify the problem and to protect the attached boundary layer from grid induced separation even if the grid spacing is much less than the boundary layer thickness (Paik 2009).

The governing equations for k-ω SST based DDES model as reported by Gritskevich *et al.* (2012) (Ansys theory guide 2010)

$$\left.\begin{aligned} &\frac{\partial \rho k}{\partial t} + \nabla.\left(\rho \vec{U} k\right) = \nabla.\left[(\mu + \sigma_k \mu_t)\nabla k\right] + P_k - \rho\sqrt{k^3}/l_{DDES} \\ &\frac{\partial \rho\omega}{\partial t} + \nabla.\left(\rho \vec{U}\omega\right) = \nabla.\left[(\mu + \sigma_\omega \mu_t)\nabla\omega\right] + 2(1-F_1)\rho\sigma_{\omega 2}\frac{\nabla k.\nabla\omega}{\omega} + \alpha\frac{\rho}{\mu_t}P_k - \beta\rho\omega^2 \end{aligned}\right\} \quad (1)$$

$$\mu_t = \rho\frac{a_1.k}{\max(a_1\omega, F_2.S)} \quad (2)$$

Where F_1 and F_2 are the blending functions.

$$F_1 = \tanh(arg_1^4) \quad (3)$$

$$\left.\begin{aligned} F_1 = arg_1 &= \min\left(max\left(\frac{\sqrt{k}}{C_\mu\omega d_\omega}, \frac{500\nu}{d_\omega^2\omega}\right), \frac{4\rho\sigma_{\omega 2}k}{CD_{k\omega}d_\omega^2}\right)\tanh(arg_1^4) \\ CD_{k\omega} &= max\left(2\rho\sigma_{\omega 2}\frac{\nabla k\, \nabla\omega}{\omega}, 10^{-10}\right) \\ F_2 &= \tanh(arg_2^2) \\ arg_2 &= \max\left(\frac{2\sqrt{k}}{C_\mu\omega d_\omega}, \frac{500\nu}{d_\omega^2\omega}\right) \end{aligned}\right\} \quad (4)$$

Where d_ω is the distance from the wall. The P_k (production term) present in the above equation is defined as follows

$$P_k = min\left(\mu_t S^2, 10.C_\mu\rho k\omega\right) \quad (5)$$

The length scale for DDES approach i.e., l_{DDES}

$$l_{DDES} = l_{RANS} - f_d\max(0, l_{RANS} - l_{LES}) \quad (6)$$

$l_{LES} = C_{DES}h_{max}$ (h_{max}= the maximum edge length of the cell) (7)

$$l_{RANS} = \frac{\sqrt{k}}{C_\mu\omega} \quad (8)$$

$$\left.\begin{aligned} C_{DES} &= C_{DES1}.F_1 + C_{DES2}.(1-F_1) \\ f_d(blending\ function) &= 1 - tanh[(C_{d1}r_d)^{C_{d2}}] \\ r_d &= \frac{\nu_t + \nu}{\kappa^2 d_\omega^2\sqrt{0.5(S^2+\Omega^2)}} \end{aligned}\right\} \quad (9)$$

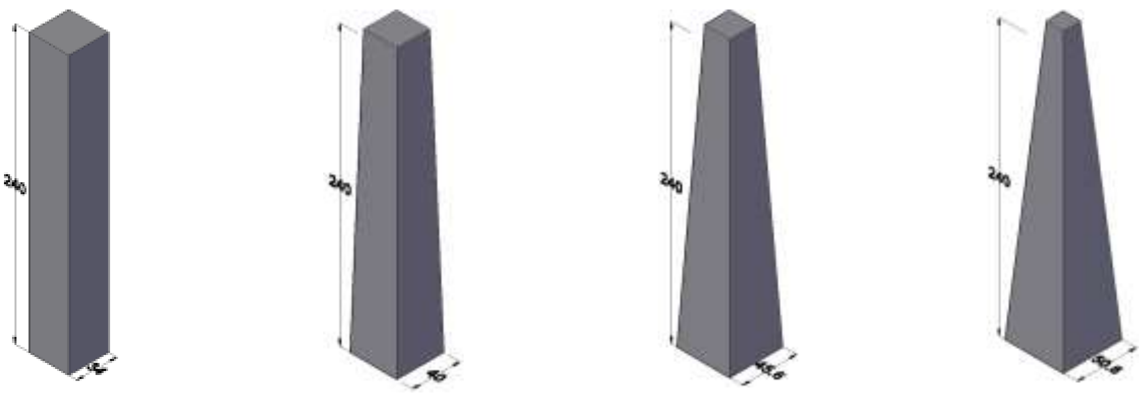

(a) (b) (c) (d)

*All dimensions are in meters.

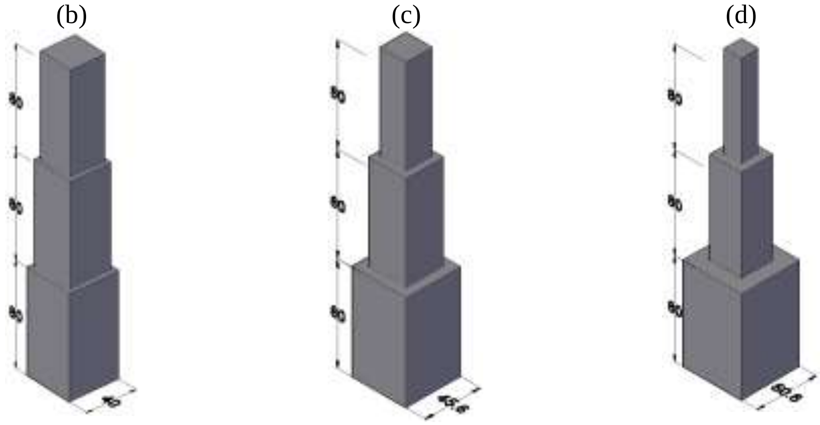

(e) (f) (g)

Fig. 1 Prototype building geometries (a)SQ, (b)TP5, (c)TP10, (d)TP15, (e)SB5, (f)SB10 and (g)SB15

Here S is the magnitude of the strain rate tensor and Ω is the magnitude of the vorticity tensor and the model constants are

C_μ= 0.09, κ=0.41, a_1=0.31, C_{DES1}=0.78, C_{DES2}=0.61, C_{d1}=20, C_{d2}=3

3.1 Geometric details of buildings

In the present investigation, the modifications are implemented on square building model keeping total volume and height as constant and customizing base and top dimensions. One reference square model and six height modified taper and set-back models (Fig. 1) are considered for the investigation of forces and pressure in along-wind and across-wind directions. The reference square and other models have an aspect ratio of 7 and side ratio as 1:1. Taper building models with 5%, 10%, 15% tapering ratios ($\mathrm{T.R.} = (\text{Bottom width} - \text{Top width})/\text{Height}$) and set-back models having top and bottom dimensions same as that of tapered models have been adopted for the numerical simulation.

For convenience, the abbreviated forms for each model are used such as SQ for square, TP5, TP10, TP15 for tapered models having 5%, 10%, 15% taper ratio and similar shorthand notations are used for set-back models i.e. SB5, SB10, SB15.

A geometric scale of 1/400 is taken for all the building models and the details of prototype geometry and dimensions are shown in Fig. 1 and Table 2 below:

3.2 Computational domain and Grid arrangement

Obtaining appropriate accuracy of the solution through numerical simulation is hugely dependent on factors such as computational domain, grid type and resolution, boundary conditions, solver settings etc. The accuracy of the results is compromised if these parameters are not controlled carefully. This section describes the computational domain, mesh scheme, boundary conditions and solution methods adopted in the present numerical simulation study.

Table 2 Details of building geometry

Model Type	Top width(m)	Middle width(m)	Bottom width(m)	Height (m)
SQ	34	-	34	240
TP5	28	-	40	240
TP10	21.6	-	45.6	240
TP15	14.6	-	50.6	240
SB5	28	35.5	40	240
SB10	21.6	31	45.6	240
SB15	14.6	27	50.6	240

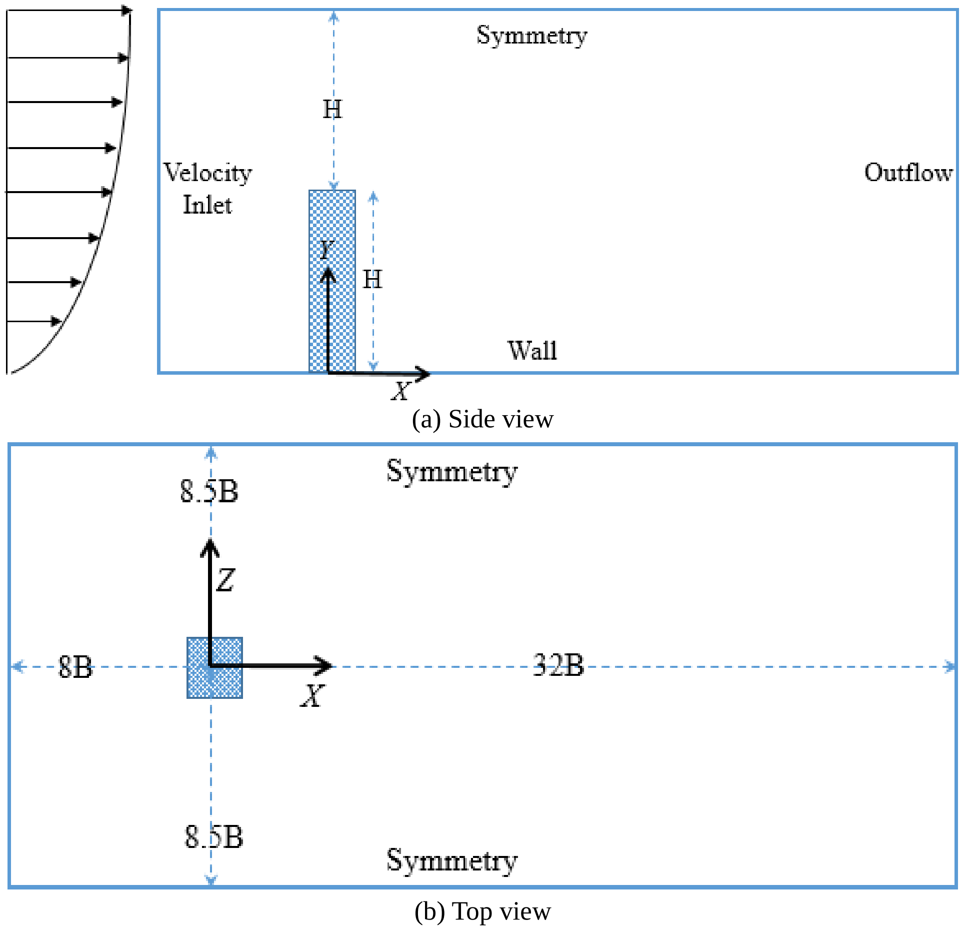

Fig. 2 Computational Domain

Concerning the size of the domain in CFD simulations, the distance between the building surfaces and corresponding domain plains should be large enough to allow the flow to develop fully and should avoid the generation of artificial acceleration in the flow. Various guidelines and recommendations have been proposed earlier (COST 2007, AIJ 2008) and can be referred for the generation of the domain. These guidelines suggest the upstream, downstream, vertical and lateral distances as 5H, 10-15H, 4-5H and 4.6-5H respectively from the building. However, Meng *et al.* 2018, Zhao and He 2017, Mou *et al.* 2017 and Huang et al. 2007 recommended these distances as 1-1.5H, 2.-2.5H, 2-2.5H and 6B in upstream, downstream, vertical and lateral directions respectively. The present study adopts the arrangement of computational domain recommended by Huang *et al.* (2007), which also manages the blockage ratio to be less than 5% and wall effects are eliminated. The size of the computational domain is shown in Fig. 2. The total length of computational domain in a stream-wise direction (X-direction) is 40B (5.7H) (B is the width of the building at the base), in span-wise or Z-direction 17B (2.4H) and height of the domain is 2H (H is the height of the building). The size of the domain and positioning of the building in the domain ensures that there is no hindrance effect of the domain boundaries on the building model.

The quality of the grid determines the computational accuracy of the solution and convergence. So depending on the type of problem, selection of the correct grid is an important step. Generally, two types of grids i.e., structured grid and unstructured grids are widely accepted by the researchers in the field of computational wind engineering. Since the structured grids are well aligned with the domain boundary, it attenuates the problem of stress-concentration at the vicinity of boundary areas unlike unstructured grids, and moreover structured grids provide better computational efficiency over unstructured grids (Zhao and He 2017). The DES approach requires coarser mesh in RANS region (attached boundary layer) and fine mesh LES region (separation region) (Yan and Li 2017). So the computational domain around all the building models is discretized accordingly using structured grids as shown in Fig. 3. The mesh is generated around the building using Ansys/ICEM. The mesh size near the building façade and ground surface is kept fine to capture all the minute details of flow

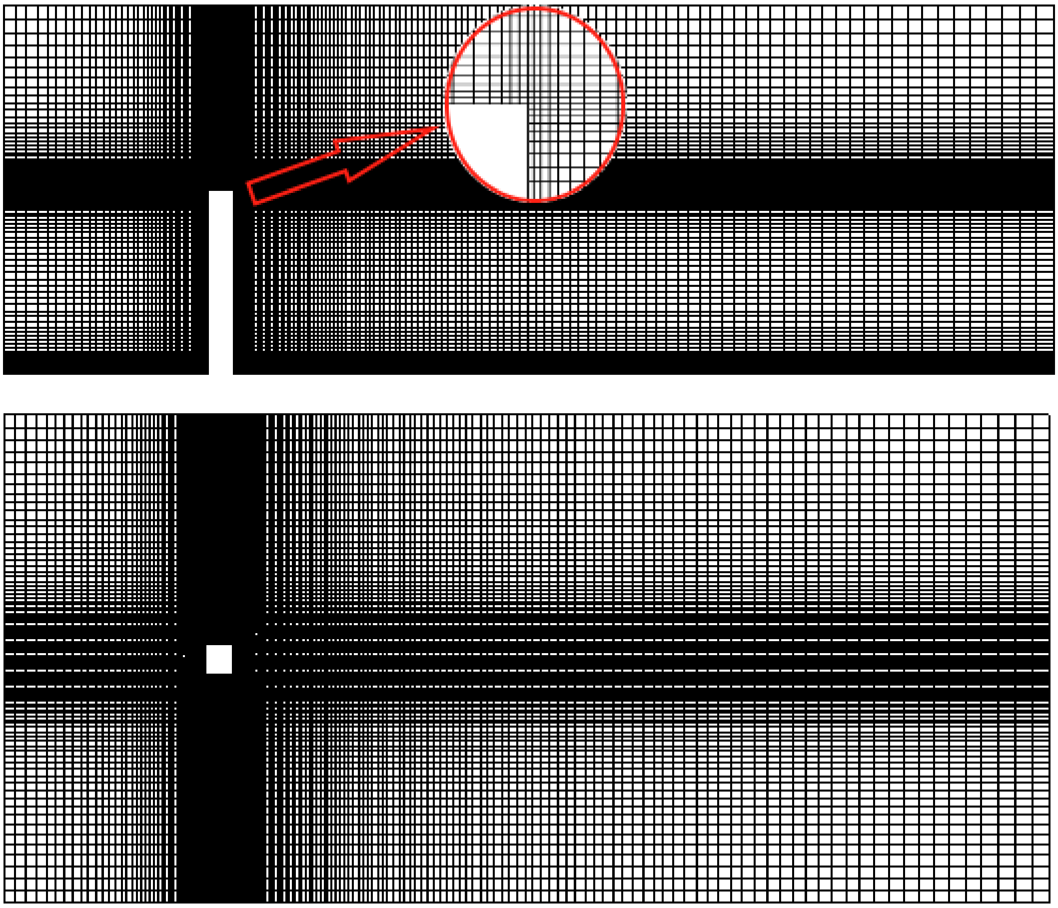

Fig. 3 Grid arrangement in vertical and plan view

characteristics (Murakami 1998), having first call height as B/1000 and growth factor of 1.05 near the building surface, a large grid stretching ratio often results in numerical oscillations, so the grid stretching ratio near the building model is kept as 1.05 (Spalart 2001) to avoid the numerical oscillations as described by Murakami (1998) and away from the building a growth factor of 1.2 is adopted.

3.3 Turbulence model and boundary conditions

The mean incident velocity of approaching boundary layer influences the mean wind loads and turbulence intensity affects the fluctuating components of loads so it is very important to model the velocity and turbulence profile correctly at the inlet of the computational domain to simulate the aerodynamic characteristics accurately (Huang *et al.* 2007). This part presents the adopted boundary conditions for the simulation.

The atmospheric boundary layer profile simulated in the wind-tunnel experimentation is in the following form of a power law

$$\frac{V}{V_o} = \left(\frac{Z}{Z_o}\right)^{\alpha} \tag{10}$$

Where V_o is the reference velocity at the reference height (Z_o) of the building i.e., 9.6 m/sec in the present case and α is the power law exponent which is 0.20. The power law wind profile used in the experimentation is introduced in the CFD simulation through UDF (user defined function) and shown in Fig. 4(a). The turbulence intensity plays an important role in flow separation and wake characteristics.

3.4 Numerical algorithm

The turbulence intensity profile (AIJ 2008) (Eq. (6)) used is shown in the Fig. 4(b) and calculated as follows

$$\frac{I}{I_o} = \left(\frac{Z}{Z_o}\right)^{-0.05-\alpha} \tag{11}$$

The DDES approach based on the SST $k-\omega$ turbulence model is adopted and the profiles of turbulent kinetic energy (k) and specific rate of dissipation (ω) (Eq. (7) and Eq. (8)) were introduced through UDF at inlet and the profiles of these parameters are shown in Figs. 4(c) and 4(d).

$$k = {}^{3}/_{2}\,((I(z).U(z))^2 \tag{12}$$

Table 3 Boundary conditions of computational domain

Inflow boundary	Velocity, turbulence intensity, k and ω	Profiles at the inlet
Downstream boundary	Outflow	$\frac{\partial}{\partial x}(u, v, w, k, w) = 0$
Top face and side faces of the domain	Free slip/ symmetry	$\frac{\partial u}{\partial y} = \frac{\partial u}{\partial w} = v = w = 0$
Bottom boundary	Wall/No slip	$u = v = w = 0$

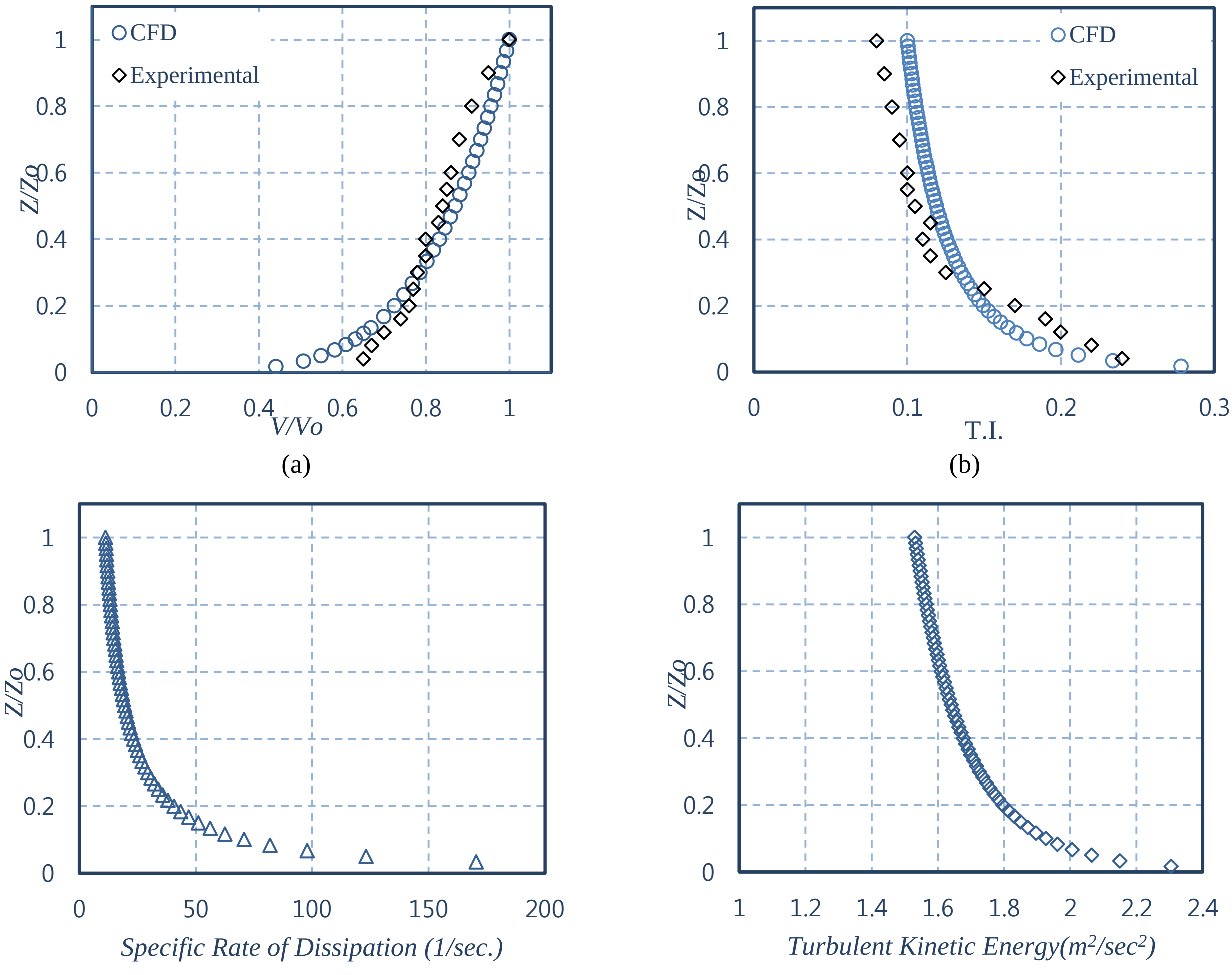

Fig. 4 Profiles of different parameters (a) Velocity, (b) Turbulence intensity, (c) Specific rate of dissipation and (d) Turbulent kinetic energy

$$\omega = \frac{1}{C_\mu} \cdot \frac{\varepsilon}{k} \tag{13}$$

The outlet of the domain is set as zero static pressure.

The side and top faces of the domain were provided with symmetry boundary condition, which indicates the zero gradient of all the parameters (Table 3), although Mochida *et al.* (2002) and Liu and Niu (2016) have confirmed that the wall and symmetric boundary conditions provided on the side and top faces of the domain have the same effect on the solution. Building surfaces and domain bottom were assigned with no-slip boundary condition.

Table 4 Numerical schemes used in DDES

Parameter	Type
Time discretization	Bounded second order implicit
Momentum Discretization	Bounded central difference
Pressure discretization	Second order
Pressure-velocity coupling	PISO
Under-relaxation factors	0.3 for pressure and 0.7 for momentum
Turbulent kinetic energy	Second order
Turbulent dissipation rate	Second order
Pressure gradient approximation	Green-gauss cell based

In the present study, ANSYS/Fluent 17.0 CFD tool is used for numerical simulation of the problem which uses finite volume method for discretization of governing equation. Pressure based Pressure Implicit with Splitting of operators (PISO) segregated algorithm is introduced for pressure-velocity calculations, that involves one predictor and two corrector steps (Yan and Li 2017). The other schemes used for the numerical simulation are listed in Table 4.

Time step size (Δt) of 0.002 is selected. All the results are averaged and sampled after 3.0 sec. flow time from initialization of computation. First, the converged flow field is obtained from SRANS model which is later used for the initial flow conditions for DES simulation for better convergence of the simulation, the turbulence fluctuation at the inlet boundary were generated by vortex method. The convergence criteria for continuity is 10^{-5} and 10^{-4} for other parameters.

4. Definition of forces, moments and pressure coefficients

The mean and fluctuating coefficients forces and moments are defined by as follows

$$\bar{C}_{F_x} = \frac{\bar{F}_x}{0.5\rho A {U_H}^2} \qquad C_{Fxrms} = \frac{{F_x}'}{0.5\rho A {U_H}^2}$$

$$C_{Fyrms} = \frac{{F_y}'}{0.5\rho A {U_H}^2}$$

Where, $\bar{F}_x$, $\bar{F}_y$ are the mean forces in along-wind and across-wind directions, ${F_x}'$, ${F_y}'$ are the fluctuating forces, $\bar{M}_x$, $\bar{M}_y$ are the mean overturning moments in two directions, ${M_x}'$, ${M_y}'$ are the fluctuating components of overturning moments.

The mean wind pressure coefficients on the surfaces of the building are being calculated with the following expression

$$\overline{C_p} = \frac{\bar{P} - P_{stat}}{\frac{1}{2}\rho {U_H}^2}$$

Where, $\bar{P}$ is the mean wind pressure, P_{stat} is the static pressure at a reference height, ρ is the density of air, U_∞ is velocity at the reference height which is 9.6 m/sec at building height.

5. Results and analysis

5.1 Grid independence test

To confirm the solution to be independent of grid density, grid independence test is required. Total 8 cases of different grid arrangements and time step sizes (Δt) were tested for the square model at the normal incidence angle, and the boundary conditions for all the arrangements were kept same, the details of grids is provided in Table 5.

As the DDES approach requires the finer mesh in the separated region especially in the leeward direction of the building and uses LES mode to resolve the flow, So non-dimensional wall distance Y^+ ($=u^* y/\vartheta$, where u^* is friction velocity at nearest wall, ϑ is local kinematic viscosity and y is the first cell distance from wall) <5 is preferable. Three grids with first cell height B/1000, B/750 and B/500 are taken for the test. Liu and Niu (2016) analyzed the effect of time step size on flow features and found that 0.005 is the optimal value of time step and below this, there is no major influence on the results. Nevertheless, as among all grids, the arrangement with first cell height as B/1000 shows Y^+ <5 (Table 5), this grid is tested for the influence of time step size (Δt) with four time steps i.e.. 0.001, 0.002, 0.005 and 0.01 and among these the grids with B/1000 as minimum grid size and Δt as 0.002 is adopted for all the simulations to achieve the accuracy of the results.

Obasaju (1992) in his experimentation found irregular changes in the drag values and suggested that a longer time is needed to achieve more accuracy in the results. So, considering this factor, in the present case each simulation is averaged over 7s flow time.

5.2 Aerodynamic force analysis

Prior to obtaining computational results, the experimental tests were performed to assess the accuracy of the simulation. Fig. 6 shows the comparison chart of mean and RMS along wind forces for all the models at 0^o angle of incidence. All the mean and RMS coefficients are calculated with the help of expressions provided above. The experimental and CFD results are compared in the same chart. As compared to the experimental values the results obtained from the numerical simulation are underpredicted little bit. From the comparison charts, it is observed that the increase in taper ratio or modification for tapered and set-back models the mean and RMS values of along-wind forces suppress gradually and this suppression is more pronounced for set-back models rather than tapered models. The tapered and set-back models with 15% taper ratio show maximum suppression in mean and RMS force coefficients.

Table 5 Mesh description for DDES cases

Case	Mesh numbers (millions)	Minimum grid size	Turbulence model	Time step size (Δt)	Y$^+$	$\bar{C}_D$	C_{Drms}	C_{Lrms}
1	3.5	B/1000	DDES	0.001	<5	1.28	0.31	0.43
2	3.5	B/1000	DDES	0.002	<5	1.28	0.27	0.43
3	1.8	B/1000	DDES	0.002	<5	1.23	0.33	0.39
4	2.1	B/1000	DDES	0.002	<5	1.24	0.25	0.40
5	3.5	B/1000	DDES	0.005	<5	1.33	0.23	0.41
6	3.5	B/1000	DDES	0.01	<5	1.27	0.19	0.45
7	3.5	B/750	DDES	0.002	>5	1.29	0.26	0.38
8	3.5	B/500	DDES	0.002	>5	1.25	0.26	0.42

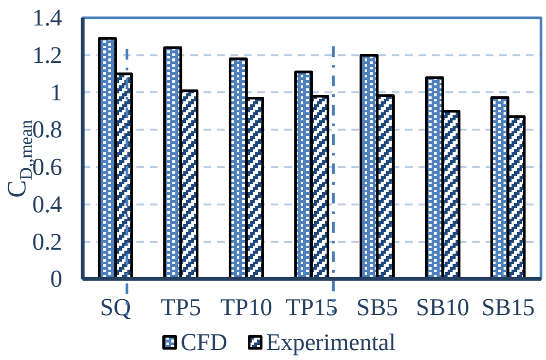

(a)

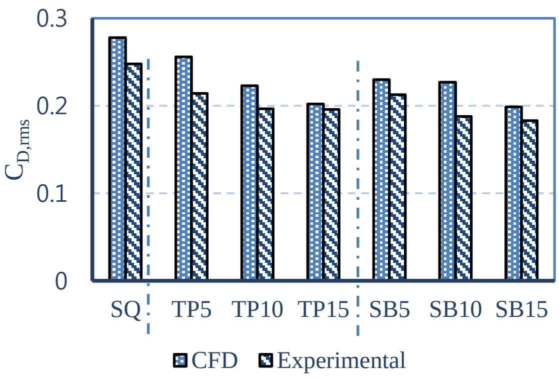

(b)

Fig. 6 Variation of along-wind forces with respect to the square building (a) $\bar{C}_D$ and (b) C_{Drms}

On the basis of comparison between experimental and computed results, it is reasonable to draw the conclusion that absolute error in mean and RMS forces with respect to experimental results is less than 14% and 12% respectively, which is under the acceptable limit.

The mean across-wind load on a symmetrical body is theoretically zero for normal wind incidence, so, only RMS across-wind loads are discussed here for all the building models. Fig. 7 below depicts the comparison of RMS across-wind forces on square and height modified tapered and set-back models for zero degrees angle of incidence. The across-wind fluctuating forces on the buildings are generated by the separation of the shear layer from the leading edges of the building and formation of alternate vortex shedding. The vortex shedding frequency is a function of the width of the building and Strouhal Number (*St* = f.B/U, where f is the frequency of shedding, B is the width of the building in across-wind direction and U is the reference velocity). Unlike a square building, the cross-sectional area (and so the width) of the taper and setback building reduces along the height which consequently outspread the vortices over a broad range of frequencies and constraints the vortices to shed with different frequencies along the elevation of the building. This phenomenon breaks the coherency between the vortices and so a reduction of resultant fluctuating across-wind forces is obtained. This hypothesis can be affirmed by observing the variation of RMS across-wind force in Fig. 7. The RMS across-wind forces also reduce due to tapering and set-back treatment.

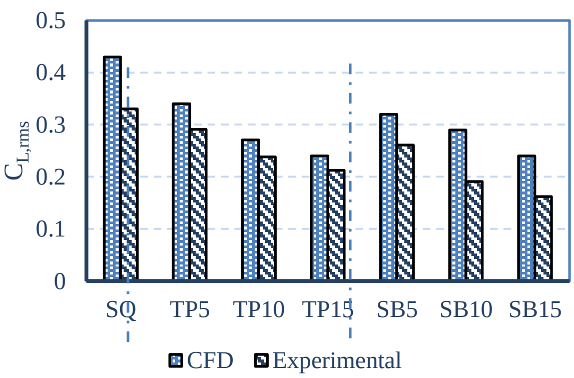

Fig. 7 Variation of RMS across-wind forces (C_{Lrms}) with respect to square building

The logical aspect of set-back model being more effective than tapered one in reduction of the mean along-wind force can be understood with the fact that, the area in the upper portion of set-back models is lesser than tapered

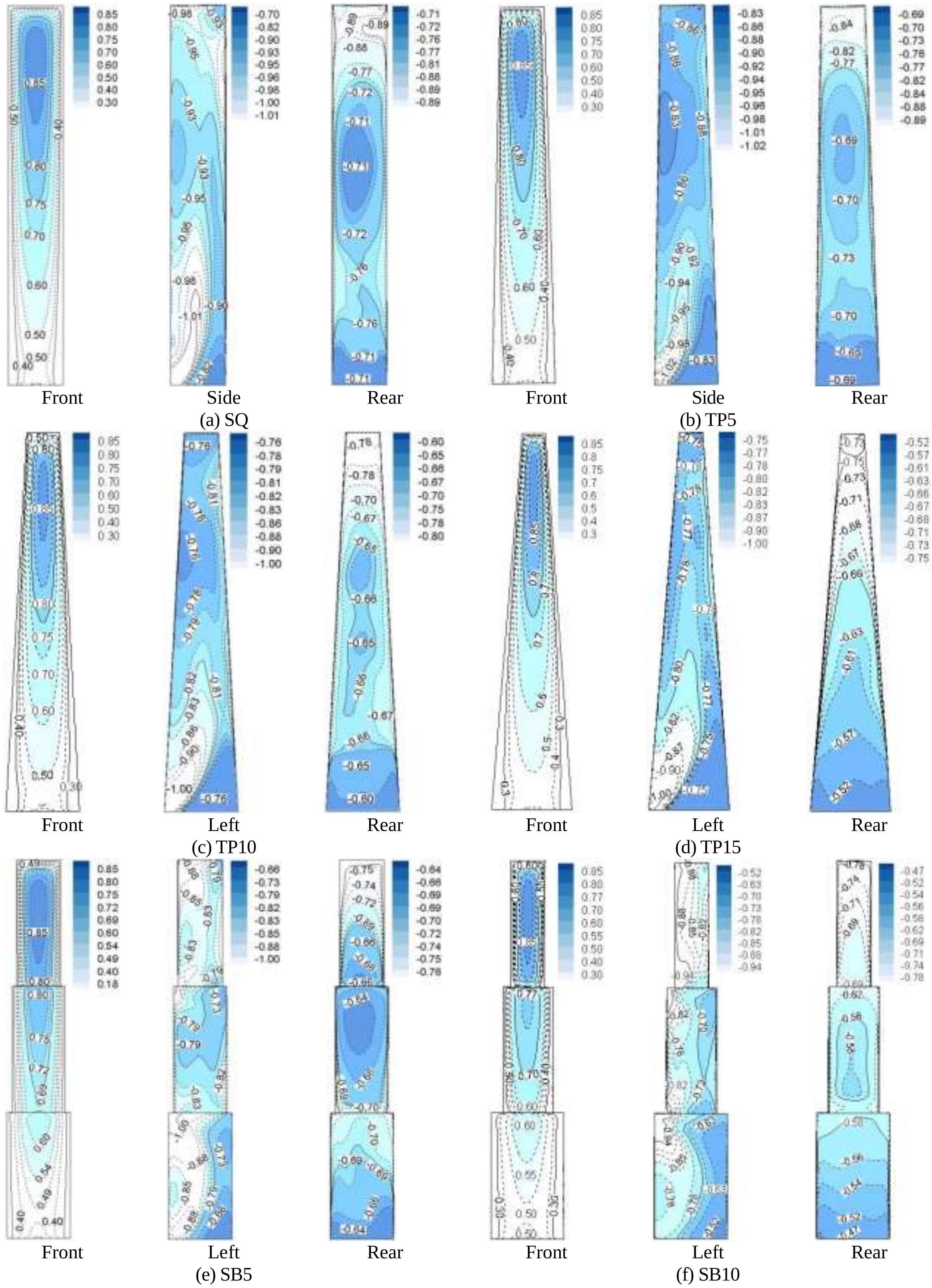
Front
Side
Rear
(a) SQ
Front
Side
Rear
(b) TP5
Front
Left
Rear
(c) TP10
Front
Left
Rear
(d) TP15
Front
Left
Rear
(e) SB5
Front
Left
Rear
(f) SB10

Continued-

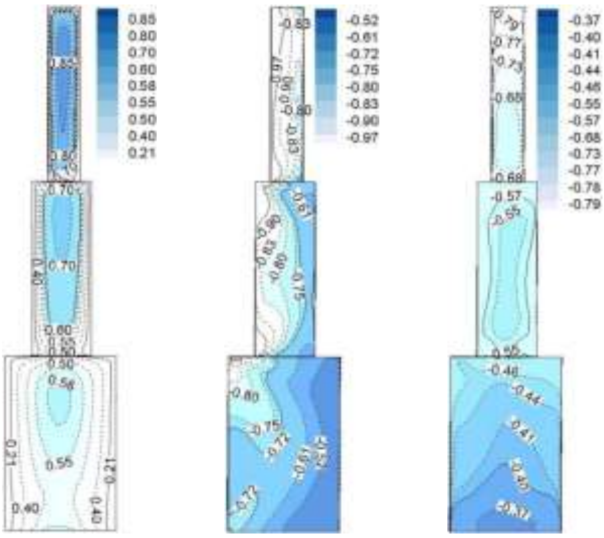

Front Left Rear
(g) SB15

Fig. 8 Variation of mean pressure coefficients ($\bar{C}_P$) on the surfaces of buildings (a)SQ, (b)TP5, (c)TP10, (d) TP15, (e) SB5, (f) SB10 and (g) SB15

model, the high-speed wind in the upper region of the boundary layer interacts with the lesser area of the set-back building and consequently the mean along wind force is reduced. A better comprehension of the mechanism of reduction in mean forces can be acquired by analyzing the flow field around the buildings (discussed in the later section of the paper).

5.3 Pressure distribution

Existing studies have demonstrated that the distribution of the pressure on the surfaces of the building highly depends on the geometric shape of the building (Kim and Kanda 2013, Bandi *et al.* 2013, Tanaka *et al.* 2012) and limited studies have discussed the distribution and pressure sensitivity of tapered and set-back buildings. This section discusses the variation of the mean coefficient of pressures (C_{Pmean}) on the surfaces of square and aerodynamically modified buildings.

The distribution pattern of C_{Pmean} contours on the surfaces of all the seven models is presented in Figs. 8 and 9 depicts the variation of the mean pressure coefficient along the periphery of the building at three height levels i.e., H/6, H/2 and 5H/6.

It is observed from both the figures that the maximum value of the mean pressure coefficient on the windward faces of all the buildings are almost the same and there is no significant change in the maximum value.

The cross-sectional dimension of the height modified models reduces along the height so it can be seen that the contour area of maximum pressure coefficient is reduced and this reduction increases as the taper ratio is increased. However, the distinction of pressure pattern is observed on the side and leeward faces between seven building models. On the side and leeward surfaces, as the modification length is increased the negative value of the pressure reduces (less negative) or moves towards positive pressure. The variation of the pressure on leeward surfaces vary largely from bottom to top of the height modified models than reference square model. The mean values of pressure coefficients at the bottom of tapered and set-back models are lesser at bottom side than the square model and larger values are observed at the top sections as compared to the square model. Kim and Kanda (2013) also observed such kind of pattern and presented their argument on it. According to the authors such distribution of the pressure is produced due to the fact that, the height modified taper and set-back models are having increasing dimensions along the bottom, which hampers the downwash from upper portion of the geometry and reduces the speed of downwash, on the other hand, the upward flow diverged from the stagnation point on the windward face of the building gets accelerated due to the lesser cross-section along the upward direction.

The square and tapered models seem to have one stagnation point on the windward face of the building while the set-back models interestingly observed to have three stagnation points at each step, which reveals that all the three steps of the set-back buildings are influenced by different vortex and having different properties.

As discussed in the previous section, the mean along-wind forces are reduced as the taper ratio is increased, and set-back models are more efficient in the reduction of mean forces as compared to tapered one. The reason behind such pattern of reduction in forces due to aerodynamic treatments can be perceived by examining the variation in pressure on windward and leeward surfaces of the buildings along the periphery of the building models at three levels (Fig. 9).

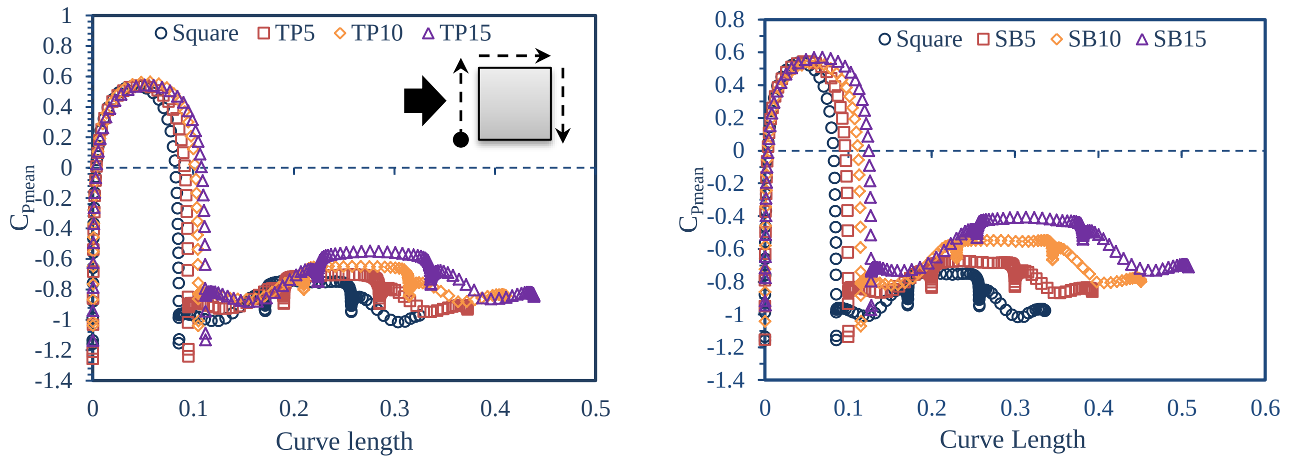

(a) H/6

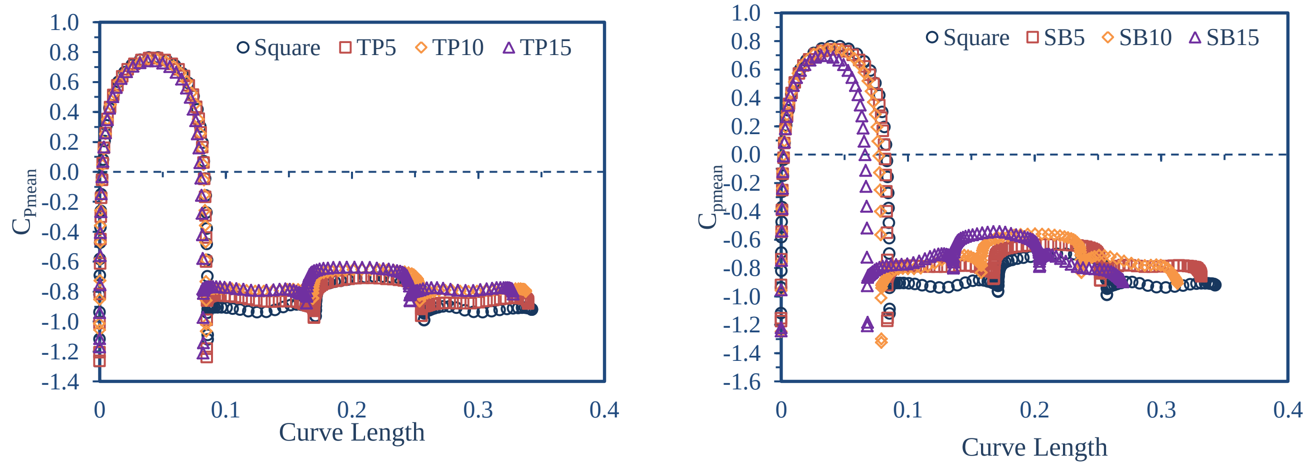

(b) H/2

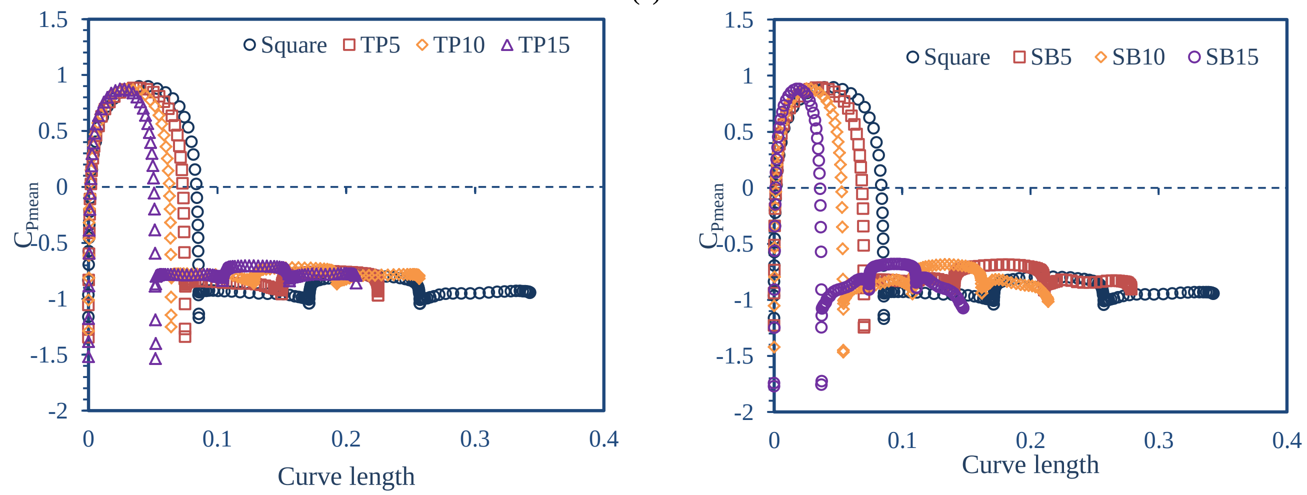

(c) 5H/6

Fig. 9 Variation of mean pressure coefficient along periphery at three height levels (a) H/6, (b) H/2 and (c) 5H/6

For taper and set-back models, the influence of the shape on positive mean pressure exerted on windward wall is insignificant as compared to square model, but the leeward side experiences the increase in pressure (or less negative pressure) and the pressure further becomes less negative with increase in modification length, which consequently provides less drag on the modified models, the better insight of this phenomenon can be acquired by observing the flow pattern around the buildings which is discussed in the last section of this paper.

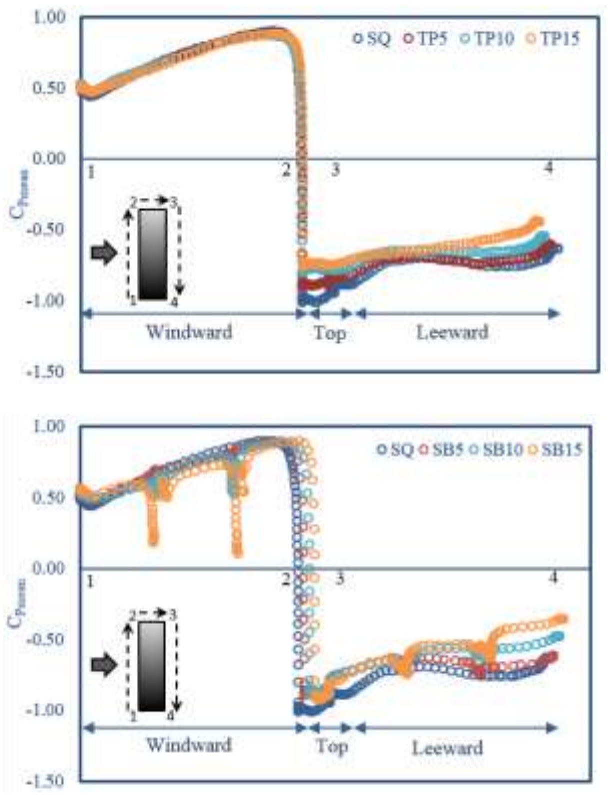

Fig. 10 Comparison of Local C_{Pmean} along the vertical centre line building models (a) Taper and (b) Set-back

The reattachment of flow on the side faces of the building can be recognized by analyzing the variation of mean pressure on these surfaces from leading to trailing edge, the recovery of pressure confirms the reattachment of the flow on the side faces of the building (Robertson *et al.* 1978, Kim and Kanda 2013). The above-mentioned condition is examined for three height levels at H/6, H/2 and 5H/6 (Fig. 9). At H/6 height level, the mean pressure recovery on the side faces is observed for all the building models but all the set-back models show more recovery at this height than tapered models, it implies that the reattachment of flow may occur at this height level for all the models. For H/2 level, the tapered and square models do not show any recovery in pressure, unlike set-back model. As the taper ratio of set-back models is increased the recovery of pressure is more pronounced and SB15 is having maximum gain in the pressure at trailing edge of the building and it implies that degree of reattachment is high for the SB15 model. A similar pattern of pressure gain is observed at 5H/6 height levels.

Fig. 10 displays the variation of mean C_p on the central axis of the windward, top and leeward surfaces. As evident, the mean C_p on windward surface of the square and all tapered models are overlapped, showing that the wind pressure on windward façade does not get disturbed significantly by providing a taper to the building. The maximum mean value of pressure coefficient achieved for SQ is 0.9 at 0.5 m height (scaled height) while TP5, TP10, TP15 experience 0.88 as maximum pressure coefficient at 0.48 m. Meanwhile, all the set-back models exhibit an abrupt drop of mean C_p at each step. Each step behaves individually that is why we can see separate stagnation point for each step of the building. The maximum value on the windward face for SB5, SB10 and SB15 are 0.9 at the height 0.5 m. The C_{Pmean} on the leeward surface of the buildings is compared in same Figs. 10(a) and 10(b).

If we observe closely the leeward pressure coefficients of all the models, the top portions of the buildings do not show a large difference in the mean pressure coefficients, however, the pressure seems to be more recovered as we move towards the foot of the buildings. Higher modifications i.e., TP15 and SB15 show the highest recovery and the difference between the top and bottom of the building (as discussed previously) pressure increases as the tapering ratio is increased.

6. Flow visualization

The vortices formation from the sides of the building and the fashion in which the separated vortices are introducing themselves into the wake region, determine majorly the nature of mean and dynamic components of forces in either direction.

Due to the intricacies and possible large variations in the flow configurations in the flow field, the physical mechanism behind the variation in load distribution due to change in shape of the building cannot be achieved through present level of understanding, CFD analysis provides comprehensive characteristics of the physical processes a turbulent flow is going through during the interaction with the building.

This section discusses the flow field behaviour around the square, tapered and set-back buildings. Fig. 11 shows the mean streamlines and velocity contours in X-Y vertical midplane and X-Z horizontal planes at three height levels i.e., H/6, H/2, 5H/6. To comprehend the differences in the flow features between square and tapered buildings tapered and set-back models with 10% modification lengths (i.e., TP10 and SB10) are adopted.

As discussed above, all the flow regimes formed due to the interaction of wind and structure can be observed in Fig. 11, the formation of the frontal vortex can be recognized in Figs. 11(a)-11(c) in vertical midplanes at the upstream foot and at each step of the set-back building (marked by a red circle). The velocity contours and mean streamlines in vertical midplanes show that the reattachment length for the tapered and set-back model is increased with respect to square model and recirculation regime is more stretched towards the downstream direction for modified buildings, with set-back having a larger extension than other two. There is no reattachment of the flow on the top of the buildings for all the cases and separation bubble at the top is more elongated in case of tapered and set-back models. The flow separates from the sides of the building and there is the formation of two counter-rotating vortices in the downstream of the building and is shown in the X-Z horizontal planes at three levels of height along Z-direction.

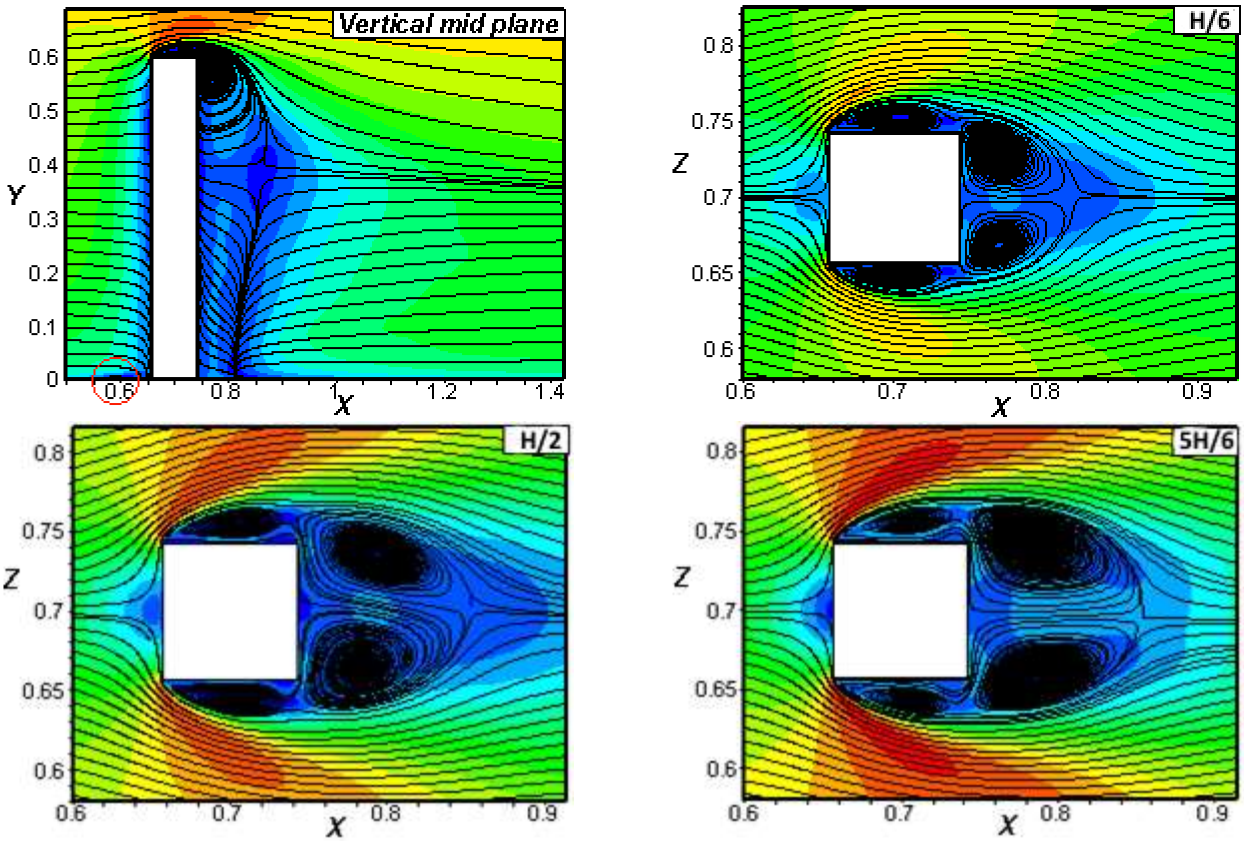

(a)

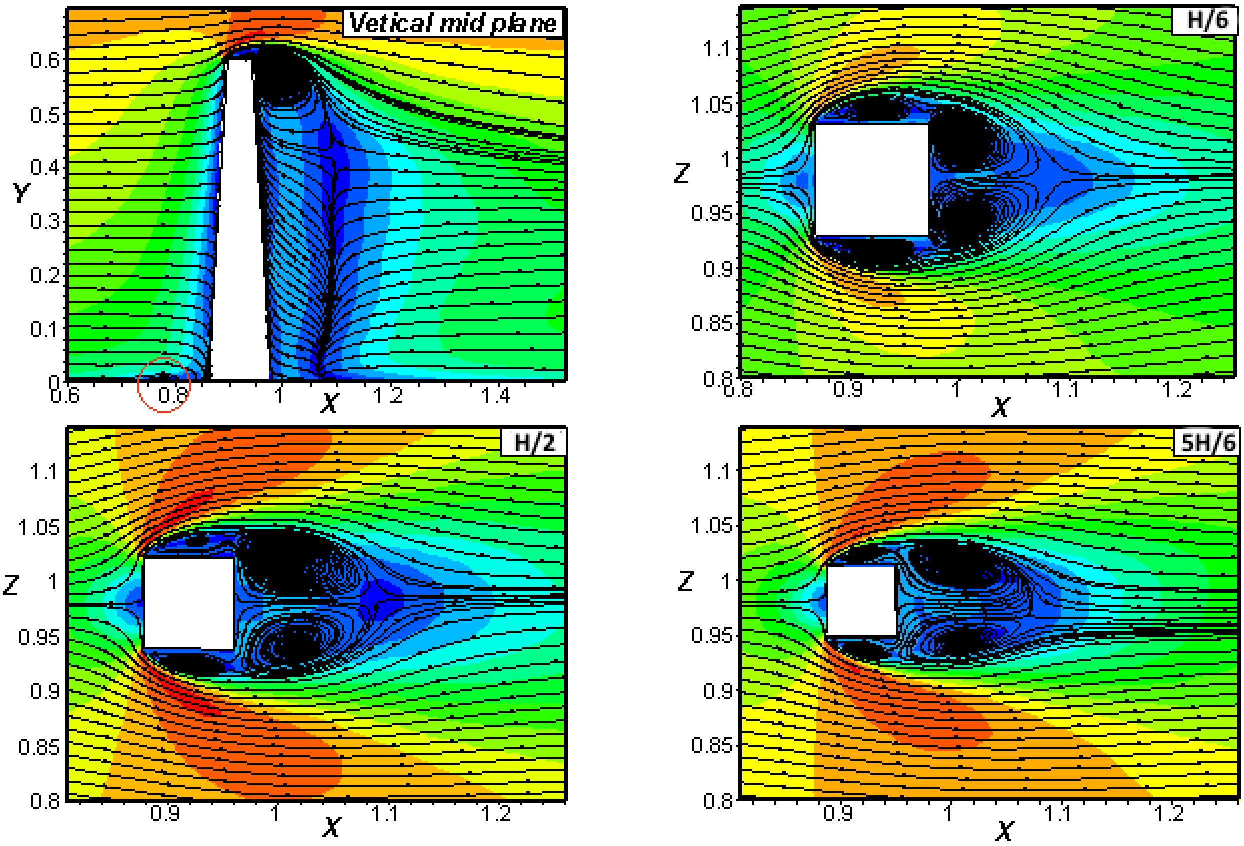

(b)

Continued-

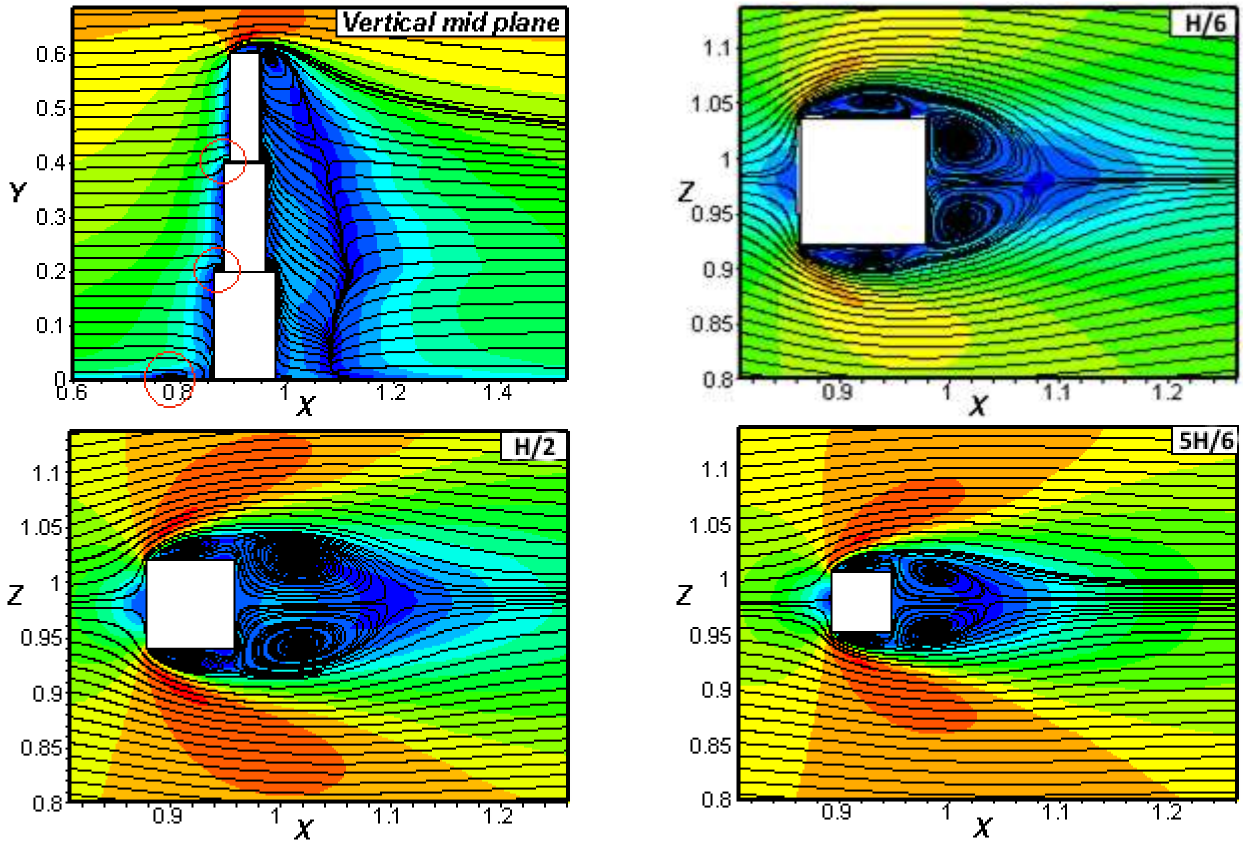

(c)

Fig. 11 Mean flow stream lines and flow field in X-Y mid plane, three height levels in X-Z planes i.e., H/6, H/2, 5H/6 (a) SQ (b) TP10 (c) SB10

In the field of wind engineering generally, two types of turbulence are considered in the study of the aerodynamics of a bluff body. One, which is present in the incident wind and other is signature turbulence or body induced turbulence (Kim and Kanda 2010a). The signature turbulence from the body is responsible for the generation of vortices and its properties and vortex shedding from the sides of the building leads the diffusion of momentum into the wake behind the building. The higher the signature turbulence lesser will be the width and length of the wake region. Going by this logic and observing the present flow structures, indicates that as the modification is provided to the square building, the production of body induced turbulence motivated by the geometry of the building decreases and there is less diffusion of momentum behind the building which leads to the elongation of separated region and reattachment length on the ground (Elkhoury 2016, Shirzadi *et al.* 2017).

Now if we look at the transverse width of the wake, it decreases along the elevation of the building for height modified models, vortices become flatter and stretched towards the downstream direction as compared to reference square model. The elongation of vortices leads the recovery (less negative) of pressure on the leeward surface of the building which reduces the overall drag force on the aerodynamically treated buildings (Huang *et al.* 2007).

7. Conclusions

The present study on aerodynamic treatment of tall buildings with taper and set-back modifications analyzes the characteristics of wind-induced forces and flow field around the modified buildings.

To avoid the loss of usable area due to aerodynamic modifications, the volume of all the buildings is kept constant by keeping the height of the building same and customizing other dimensions. Three tapering ratios are used for tapered buildings i.e., 5%, 10%, 15% and three set-back models with top and bottom dimensions same as that of tapered models are adopted. Computational fluid dynamics analysis is carried out by using Delayed Detached-eddy Simulation as this approach is proved to provide satisfactory results for the flows encountering massive separation. After examining all the results following conclusions are drawn:

- The mean/ RMS along-wind and across-wind forces are mitigated with the application of the tapering and set-back aerodynamic treatments, but the set-back modifications are more worthwhile than tapered showing a significant reduction in the forces.
- The potential of the modification increases as the modification length is increased.

- The maximum mean pressure coefficients on the windward faces of the square, tapered and set-back models are observed not to be having a significant difference, however set-back models show an abrupt change in the pressure at the foot of each step and each step is having individual stagnation point. The contour area of maximum pressure coefficient reduces as the tapering ratio is increased.
- The mean pressure coefficient on the leeward face of the buildings recovers more as the taper ratio is increased and consequently the net along-wind force is reduced.
- The side surfaces of all the building models show different pressure distribution.
- The mean flow field around the square, TP10 and SB10 building models are analyzed and the physical significances of different flow regimes are discussed.

References

Asghari, M. and Kargarmoakhar, R. (2016), "Aerodynamic mitigation and shape optimization of buildings : Review", *J. Build. Eng.*, **6**, 225-235. https://doi.org/10.1016/j.jobe.2016.01.009.

ANSYS Fluent 13.0 theory guide, turbulence, ANSYS Inc. Canonsburg, PA, 2010.

Bandi, M., Tanaka, H., Kim, Y.C., Ohtake, K., Yoshida, A. and Tamura, Y. (2013), "Peak pressures acting on tall buildings with various configurations", *Int. J. High-rise Build.*, **2**, 229-244.

Bunge, U., Mockett, C. and Thiele, F. (2007), "Guidelines for implementing detached-eddy simulation using different models", *Aerosp. Sci. Technol.*, **11**(5), 376-385. https://doi.org/10.1016/j.ast.2007.02.001.

COST (2007), Best Practice Guideline for the CFD Simulation of Flows in the Urban Environment COST Action 732.

Deng, T., Fu, J.Y., Xie, Z.N., Pi, Y.L. and Shi, B.Q. (2018), "An experimental study on the wind pressure distribution of tapered super high-rise buildings", *Struct Des. Tall Spec. Build.*, **27**, 1-11. https://doi.org/10.1002/tal.1483.

Deng, T., Yu, X. and Xie Z. (2015), "Aerodynamic measurement of across-wind loads and responses of tapered super high-rise buildings", *Wind Struct.*, **21**(3), 331-352. http://dx.doi.org/10.12989/was.2015.21.3.331.

Elkhoury, M. (2016), "Assessment of turbulence models for the simulation of turbulent flows past bluff bodies", *J. Wind Eng. Ind. Aerod.*, **154**, 10-20. https://doi.org/10.1016/j.jweia.2016.03.011.

Gritskevich, M.S., Garbaruk, A.V., Schutze, J. and Menter, F.R. (2012), "Development of DDES and IDDES formulations for the $k-\omega$ shear stress transport model", *Flow Turbul. Combust*, **88**(3), 431-449.

Huang, H., Li Q.S. and Xu, S. (2007), "Numerical evaluation of wind effects on a tall steel building by CFD", *J. Constrct. Steel Res.*, **63**(5), 612-627. https://doi.org/10.1016/j.jcsr.2006.06.033.

Haupt, S.E., Zajaczkowski, F.J. and Peltier, L.J. (2011), "Detached eddy simulation of atmospheric flow about a surface mounted cube at high Reynolds number", *J. Fluids Eng.*, **133**(3), 0310021-0310028. doi:10.1115/1.4003649.

Irwin, P.A. (2009), "Wind engineering challenges of the new generation of super-tall buildings", *J. Wind Eng. Ind. Aerod.*, **97**(7-8), 328-334. https://doi.org/10.1016/j.jweia.2009.05.001.

Kareem, A. (1983), " Mitigation of wind induced motion Of tall buildings", *J. Wind Eng. Ind. Aerod.*, **11**(1-3), 273-284. https://doi.org/10.1016/0167-6105(83)90106-X.

Kareem, A., Kijewski, T. and Tamura, Y. (1999), "Mitigation of motions of tall buildings with specific examples of recent applications", *Wind Struct.*, **2**(3), 201-251. http://dx.doi.org/10.12989/was.1999.2.3.201.

Kim, Y. and You, K. (2002), "Dynamic responses of a tapered tall building to wind load", *J. Wind Eng. Ind. Aerod.*, **90**(12-15), 1771-1782. https://doi.org/10.1016/S0167-6105(02)00286-6.

Kim, Y.C., You, K.P. and Ko, N.H. (2008), "Across-wind responses of an aeroelastic tapered tall building", *J. Wind Eng. Ind. Aerod.*, **96**(8-9), 1307-1319. https://doi.org/10.1016/j.jweia.2008.02.038.

Kim, Y. and Kanda, J. (2010a), "Characteristics of aerodynamic forces and pressure on square plan buildings with height variations", *J. Wind Eng. Ind. Aerod.*, **98**(8-9), 449-465. https://doi.org/10.1016/j.jweia.2010.02.004.

Kim, Y. and Kanda, J. (2010b), "Effects of taper and set-back on wind forces and wind-induced response of tall buildings", *Wind Struct.*, **13**(6), 499-517. http://dx.doi.org/10.12989/was.2010.13.6.499.

Kim, Y. and Kanda, J. and Tamura, Y. (2011), "Wind-induced coupled motion of tall buildings with varying square plan with height", *J. Wind Eng. Ind. Aerod.*, **99**(5), 638-650. https://doi.org/10.1016/j.jweia.2011.03.004.

Kim, Y. and Kanda, J. (2013), "Wind Pressure on tapered and set-back tall buildings", *J. Fluid Struct.*, **39**, 306-321. https://doi.org/10.1016/j.jfluidstructs.2013.02.008.

Kim, Y., Tamura, Y. and Yoon, S. (2015), "Effects of taper on fundamental aeroelastic behaviors of super-tall buildings", *Wind Struct.*, **20**(4), 527-548. http://dx.doi.org/10.12989/was.2015.20.4.527.

Liu, J. and Niu, J. (2016), "CFD simulation of the wind environment around an isolated high-rise building: An evaluation of SRANS, LES and DES models", *Build. Environ.*, **96**, 91-106. https://doi.org/10.1016/j.buildenv.2015.11.007.

Liu, J., Niu, J., Mak, C.M. and Xia, Q. (2017), "Detached eddy simulation of pedestrian-level wind and gust around an elevated building", *Build. Environ.*, **125**, 168-179. https://doi.org/10.1016/j.buildenv.2017.08.031.

Meng, F.Q., He, B.J., Zhu, J., Zhao, D.X., Darko, A. and Zhao, Z. Q. (2018), "Sensitivity analysis of wind pressure coefficients on CAARC standard tall buildings in CFD simulations", *J. Build. Eng.*, **16**,146-158. https://doi.org/10.1016/j.jobe.2018.01.004.

Mou, B., He, B.J., Zhao, D.X. and Chau K.W. (2017), "Numerical simulation of the effects of building dimensional variation on wind pressure distribution", *Eng. Appl. Comput. Fluid Mech.*, **11**(1), 293-309. https://doi.org/10.1080/19942060.2017.1281845.

Menter, F.R. and Kuntz, M. (2004), "Adaption of eddy-viscosity turbulence models to un- steady separated flows behind vehicles", In Rose McCallen, Fred Browand, and James Ross, editors, The Aerodynamics of Heavy Vehicles: Trucks, Buses, and Trains, volume 19 of Lecture Notes in Applied and Computational Mechanics. Springer Verlag.

Murakami, S. (1993), "Comparison of various turbulence models applied to a bluff body", *J. Wind Eng. Ind. Aerod.*, **46-47**, 21-36. https://doi.org/10.1016/0167-6105(93)90112-2.

Murakami, S. and Mochida, A. (1995), "On turbulent vortex shedding flow past 2D square cylinder predicted by CFD", *J. Wind Eng. Ind. Aerod.*, **54-55**,191-211. https://doi.org/10.1016/0167-6105(94)00043-D.

Murakami, S. (1998), "Overview of turbulence models applied in CWE–1997", *J. Wind Eng. Ind. Aerod.*, **74-76**, 1-24. https://doi.org/10.1016/S0167-6105(98)00004-X.

Mochida, A., Tominaga, Y., Murakami, S., Yoshie, R., Ishihara, T. and Ooka, R. (2002), "Comparison of various k–3 model and

DSM applied to flow around a high-risebuilding – report on AIJ cooperative project for CFD prediction of wind environment”, *Wind Struct*., **5**(2), 227-244. http://dx.doi.org/10.12989/was.2002.5.2_4.227.

Mochida, A. and Lun, I.Y.F. (2008), “Prediction of wind environment and thermal comfort at pedestrian level in urban area”, *J. Wind Eng. Ind. Aerod*., **96**(10-11), 1498-1527. https://doi.org/10.1016/j.jweia.2008.02.033.

Obasaju, E.D. (1992), “Measurement of forces and base overturning moments on the CAARC tall building model in a simulated atmospheric boundary layer”, *J. Wind Eng. Ind. Aerod*., **40**(2), 103-126. https://doi.org/10.1016/0167-6105(92)90361-D.

Paik, J., Sotiropoulos, F. and Porte-Agel, F. (2009), “Detached eddy simulation of flow around two wall-mounted cubes in tandem”, *Int. J. Heat Fluid Fl.*, **30**(2), 286-305. https://doi.org/10.1016/j.ijheatfluidflow.2009.01.006.

Robertson, J.M., Wedding, J.B., Peterka, J.A. and Cermak, J.E. (1978), “Wall pressures of separation – reattachment flow on a square prism in uniform flow”, *J. Wind Eng. Ind. Aerod*., **2**(4), 345-359. https://doi.org/10.1016/0167-6105(78)90019-3.

Rodi, W. (1997), “Comparison of LES and RANS calculations of the flow around bluff bodies”, *J. Wind Eng. Ind. Aerod.*, **69-71**, 55-75. https://doi.org/10.1016/S0167-6105(97)00147-5.

Spalart, P., Jou, W., Strelets, M. and Allmaras, S. (1997), “Comments on the feasibility of LES for wings, and on a hybrid RANS/LES approach”, *Proceedings of the First AFOSR International Conference on DNS/LES*, C. Liu, USA.

Spalart, P. (2001), “Young-person's Guide to Detached-eddy Simulation for Bluff Bodies”, *NASA Center for Aerospace Information*, USA.

Strelets, M. (2001), “Detached eddy simulation of massively separated flows”, AIAA paper 2001–0879, Reno, NV.

Spalart, P.R., Deck, S., Shur, M.L., Squires, K.D., Strelets, M.K. and Travin, A. (2006), “A new version of detached-eddy simulation, resistant to ambiguous grid densities”, *Theor. Comput. Fluid Dyn.*, **20**(3), 181-195.

Spalart, P. (2009), “Detached-eddy simulation”, *Annu. Rev. Fluid Mech.*, **41**, 181-202.

Schmidt, S. and Thiele, F. (2002), “Comparison of numerical methods applied to the flow over wall-mounted cubes”, *Int. J. Heat Fluid Fl.*, **23**(3), 330-339. https://doi.org/10.1016/S0142-727X(02)00180-7.

Shirzadi, M., Mirzaei, P.A. and Naghashzadegan, M. (2017), “Improvement of k-epsilon turbulence model for CFD simulation of atmospheric boundary layer around a high-rise building using stochastic optimization and Monte Carlo sampling technique”, *J. Wind Eng. Ind. Aerod*., **171**, 366-379. https://doi.org/10.1016/j.jweia.2017.10.005.

Sharma, A., Mittal, H. and Gairola, A. (2018), “Mitigation of wind load on tall buildings through aerodynamic modifications: Review”, *J. Build. Eng*., **18**, 180-194. https://doi.org/10.1016/j.jobe.2018.03.005.

Sharma, A., Mittal H. and Gairola, A. (2019), “Detached-eddy simulation of interference between buildings in tandem arrangement”, *J. Buil. Eng.*, **21**, 129-140. https://doi.org/10.1016/j.jobe.2018.10.004.

Tanaka, H., Tamura, Y., Ohtake, K., Nakai, M. and Kim, Y.C. (2012) “Experimental investigation of aerodynamic forces and wind pressure acting on tall buildings with various unconventional configurations”, *J. Wind Eng. Ind. Aerod.*, **107-108**, 179-191. https://doi.org/10.1016/j.jweia.2012.04.014.

Tse, K.T., Hitchcock, P.A., Kwok, K.C.S., Thepmongkorn, S. and Chan, C.M. (2009), “Economic perspectives of aerodynamic treatments of square tall buildings”, *J. Wind Eng. Ind. Aerod*., **97**(9-10), 455-467. https://doi.org/10.1016/j.jweia.2009.07.005.

Tominaga, Y. and Stathopoulos, T. (2009), “Numerical simulation of dispersion around an isolated cubic building: Comparison of various types of $k-\varepsilon$ models”, *Atmos. Environ.*, **43**, 3200-3210.

Xie, J. (2014), “Aerodynamic optimization of super-tall buildings and its effectiveness assessment”, *J. Wind Eng. Ind. Aerod*., **130**, 88-98. https://doi.org/10.1016/j.jweia.2014.04.004.

Yan, B.W. and Li, Q.S. (2017), “Detached-eddy and large-eddy simulations of wind effects on a high-rise structure”, *Comput. Fluids*, **150**, 74-83. https://doi.org/10.1016/j.compfluid.2017.02.009

Zhao, X., Ding, J.M. and Suna, H.H. (2011), “Structural design of shanghai tower for wind loads”, *Procedia Eng.*, **14**, 1759-1767. https://doi.org/10.1016/j.proeng.2011.07.221.

Zhao, D. and He, B. (2017), “Effects of architectural shapes on surface wind pressure distribution: Case studies of Oval-shaped tall buildings”, *J. Build. Eng*., **12**, 219-228. https://doi.org/10.1016/j.jobe.2017.06.009.

CC